Multi-Port Converter Integrating Automatic Current Balancing Interleaved PWM Converter and Dual Active Bridge Converter with Improved Transformer Utilization

Motoki Sato
Department of Electrical and Electronic Engineering
Ibaraki University
Ibaraki, Japan
19nm633t@vc.ibaraki.ac.jp

Yoshiya Tada
Department of Electrical and Electronic Engineering
Ibaraki University
Ibaraki, Japan
18nm637l@vc.ibaraki.ac.jp

Masatoshi Uno
Department of Electrical and Electronic Engineering
Ibaraki University
Ibaraki, Japan
masatoshi.uno.ee@vc.ibaraki.ac.jp

Abstract—**Multi-port converters (MPCs) that integrate multiple converters into a single unit have been proposed to reduce the converter count in renewable energy systems where multiple power sources are employed. The conventional MPCs consisting of a dual active bridge (DAB) converter and interleaved PWM converter, however, require feedback control loops and current sensors to balance inductor currents. Furthermore, the transformer utilization in the DAB converter tends to decrease as the duty cycle of the interleaved PWM converter moves away from 0.5. This paper proposes a novel MPC integrating a DAB converter and interleaved PWM converter with an automatic current balancing capability and a high transformer utilization. Major features and fundamental operation principle are discussed. The experimental verification test using a 300-W prototype demonstrated that the proposed MPC could improve the transformer utilization and achieve an automatic current balancing.**

Keywords—Automatic current balancing; multi-port converter; interleaved PWM converter; dual active bridge (DAB) converter

I. INTRODUCTION

Recent renewable energy systems, such as photovoltaic (PV) systems, consist not only solar panels but also rechargeable batteries to smooth the unstable power generation of the solar panels. These systems tend to be complex and costly as the number of power sources increases because multiple converters are required to control each power source individually, as shown in Fig. 1(a). In order to simplify these systems, multi-port converters (MPCs) integrating multiple converters into a single unit have been proposed, as illustrated in Fig. 1(b). A PV system consisting of 48-V solar panel and 12-V rechargeable battery is focused in this paper.

MPCs are roughly divided into three groups: isolated, nonisolated, and partially-isolated MPCs. Isolated MPCs [1], [2] employs magnetic coupling using a transformer, and hence, voltages of each port can be arbitrarily determined by the transformer turns ratio. The isolated MPC topologies, however, are prone to complexity due to the large switch count because each input/output port requires multiple switches. Nonisolated MPCs reported in [3], [4] can reduce the switch count by sharing switches of two different converters. Their voltage

conversion ratios, however, cannot be arbitrarily determined by turn ratios of the transformers because of the lack of transformer.

This paper chiefly focuses on partially-isolated MPCs that can be derived from the integration of a bidirectional PWM converter and isolated converter [5], [6]. In addition to the galvanic isolation by a transformer in isolated converters, the partially-isolated MPCs can reduce the switch count by sharing switches of two converters. Several partially-isolated MPCs integrating an interleaved bidirectional PWM converter and dual active bridge (DAB) converter have been proposed in [7]–[9]. The interleaved PWM converter reduces current ripples of an input or output port and enhances a current capacity, while the DAB converter realizes bidirectional power flow with galvanic isolation and zero voltage switching (ZVS) over a wide operating range. These topologies, however, need current sensors and additional feedback control loops to balance inductor currents in the interleaved converter, increasing the system cost and complexity. Moreover, the interleaved PWM converter must operate with a high duty cycle to achieve high voltage conversion ratios (e.g., a duty cycle of 0.75 for a boost ratio of 4.0 = 48/12 V). High duty cycle operations result in not only a low-transformer utilization of the DAB converter but also increased current ripples in the interleaved converter.

This paper proposes a novel MPC integrating an interleaved PWM converter and DAB converter with a high-voltage conversion ratio and automatic current balancing capability by adding a flying capacitor to the conventional MPC. Section II presents the derivation and major features of the proposed MPC. Section III describes the operation analysis, including the current balancing principle, improved transformer
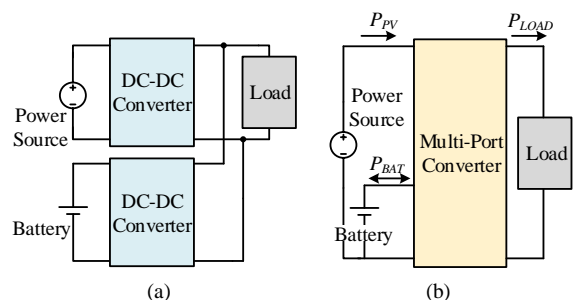

Fig. 1. (a) Traditional power system with multiple converters and (b) MPC-based system for photovoltaic system.

utilization, and ZVS range. The experimental results of a 300-W prototype will be presented in Section IV.

II. PROPOSED MPC

A. Derivation

The proposed MPC, shown in Fig. 2, is derived from the combination of an interleaved PWM converter and DAB converter together with a flying capacitor C_f. The circuit on the transformer's primary side, or a low-voltage side, consists of a two-phase interleaved bidirectional PWM converter having two switching legs. C_f is inserted between switches Q_{LB} and Q_{HB} to achieve not only an automatic capacitive current balancing but also a high voltage-conversion ratio between a battery and PV panel. The secondary side, or a high-voltage side, consists of a half-bridge rectifier with a dc blocking capacitor C_{dc} to prevent dc bias current of the transformer. C_{dc} also behaves as a voltage doubler that contributes to reducing the number of secondary winding turns.

Thanks to the integration of the two bidirectional converters, all three input/output ports are capable of bidirectional power flow. In this paper aiming for a PV system containing a rechargeable battery, the medium and low voltage ports on the primary side are assumed as a unidirectional input port for the PV panel (V_{PV}) and bidirectional port for the battery (V_{BAT}), respectively. The load port on the secondary side is a unidirectional output port (V_{LOAD}).

The proposed MPC employs PWM and phase-shift (PS) controls to regulate all input/output ports individually. The voltage conversion ratio between V_{BAT} and V_{PV} can be regulated with the PWM control manipulating duty cycles of switches Q_{LA} and Q_{LB}. The load power P_{LOAD}, on the other hand, is regulated with PS control, adjusting a phase angle φ between Q_{LA} and Q_{LC}.
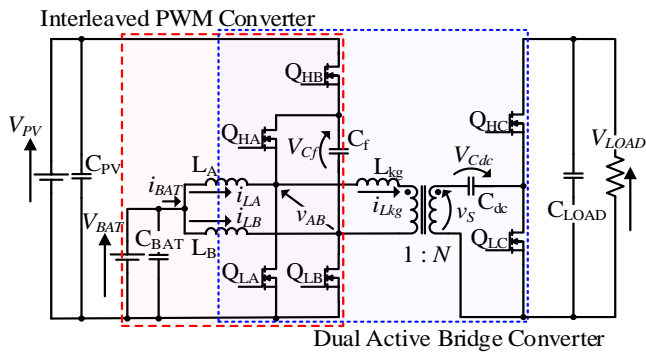

Fig. 2. Proposed multi-port converter.

B. Major Features

The voltage conversion ratio between V_{PV} and V_{BAT} (V_{PV}/V_{BAT}) at a given duty cycle is doubled compared with that of conventional MPCs consisting of a DAB converter and interleaved bidirectional PWM converter [7]–[9] because certain voltage is applied to C_f in the proposed MPC, as will be detailed in Section III-C. Consequently, the transformer utilization can be improved compared with the conventional MPC, contributing to reducing RMS currents. Moreover, the

current ripple of the battery port can be reduced as the current ripples of two inductor i_{LA} and i_{LB}, are canceled by the interleaving operation. The detailed analysis for the transformer utilization will be discussed in Section III-E.

i_{LA} and i_{LB} can be automatically balanced thanks to the charge conservation of C_f without feedback control loops nor current sensors, as will be discussed in Section III-B. Therefore, the proposed MPC can reduce circuit complexity and cost compared with that of the conventional MPCs using active current balancing techniques [7]–[9]. In addition, C_f contributes to reducing voltage stresses of switches on the primary side. The reduced switch voltage stresses would translate to not only lower conduction losses due to low on-resistances but also reduced switching losses. Furthermore, C_f reduces charge-discharge energies of inductors, contributing to an efficient power conversion as well as reduced circuit volume.

III. OPERATION ANALYSIS

The proposed MPC operates either in the battery charging mode, hybrid mode, or battery discharging mode depending on the power balance among an input power P_{PV}, battery charging power P_{BAT}, and P_{LOAD}, as depicted in Fig. 3. This paper deals only with the battery charging mode to save page length.

The key operational waveforms and current flows in the battery charging mode are shown in Figs. 4 and 5, respectively. v_{AB} and v_S are the voltages across the primary and secondary windings of the transformer, V_{Cf} and N are the voltage of C_f and transformer turn ratio, respectively. φ_D is the phase-shift duty cycle (= $\varphi/360°$), and T_S is the switching period. The switching legs of primary side, Q_{LA}–Q_{HA} and Q_{LB}–Q_{HB}, operate in an interleaved manner of 180° out of phase. The duty cycles of the low-side switches of Q_{LA} and Q_{LB} are defined as d_A and d_B respectively. Meanwhile, the duty cycle of the high-side switch Q_{LC} on the secondary side, d_C, is fixed to be 0.5. Triangular carrier waves are used to generate all gating signals. Thus, φ_D is the phase shift angle between the center of gate signals of Q_{LA} and Q_{LC}. Dead-time periods are assumed short enough to be neglected.
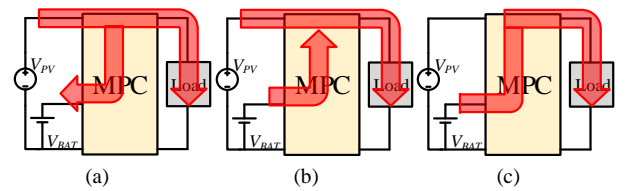

Fig. 3. Power flows in (a) battery charging mode, (b) hybrid mode, and (c) battery discharging mode.

A. Mode Analysis

The following analysis is focused on the voltages of L_A, L_B, and L_{kg} (v_{LA}, v_{LB} and v_{Lkg}) to derive P_{LOAD} and ZVS constraints. The charge and discharge currents of C_f and C_{dc} are described to demonstrate the current balancing principle in Section III-B.

Before the operational mode analysis, the voltage of C_{dc}, V_{Cdc}, is derived to determine v_S. From the average voltage at the switching node of the leg Q_{LC}–Q_{HC},
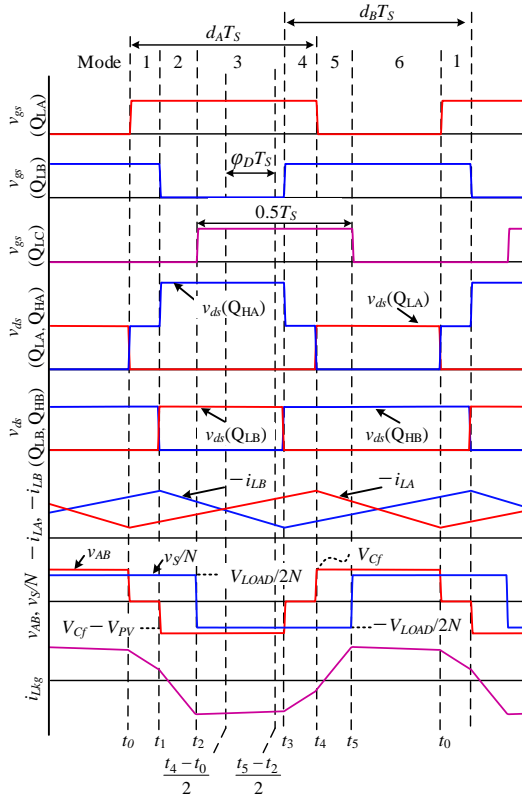
Fig. 4. Key operational waveforms in battery charging mode.

$$V_{Cdc} = (1 - d_C)V_{LOAD}, \qquad (1)$$

As aforementioned, d_C is fixed to be 0.5, hence V_{Cdc} is equal to $V_{LOAD}/2$. Therefore, v_S is $V_{LOAD}/2$ and $-V_{LOAD}/2$ during Q_{HC} and Q_{LC} are conducting, respectively.

Mode 1 (t_0–t_1) [Fig. 5(a)]: Q_{LA}, Q_{LB}, and Q_{HC} are turned on. v_{LA} and v_{LB} are expressed as

$$v_{LA} = v_{LB} = V_{BAT}. \qquad (2)$$

i_{LA} linearly increases (as well as Modes 2–4), and i_{LB} also linearly increases (as well as Modes 4–6). v_{Lkg} is $v_{AB} - v_S/N$, and therefore, it is expressed as

$$v_{Lkg} = -V_{LOAD}/2N, \qquad (3)$$

and the current of L_{kg}, i_{Lkg}, linearly decreases. In this mode, no current flows through C_f.

Mode 2 (t_1–t_2) [Fig. 5(b)]: Q_{LB} and Q_{HB} are turned off and on, respectively. v_{LB} and v_{Lkg} are expressed as

$$v_{LB} = V_{BAT} - V_{PV} + V_{Cf}, \qquad (4)$$

$$v_{Lkg} = -V_{PV} + V_{Cf} - V_{LOAD}/2N. \qquad (5)$$

i_{LB} and i_{Lkg} linearly decrease in this mode. C_f is discharged by $i_{LB} + i_{Lkg}$.

Mode 3 (t_2–t_3) [Fig. 5(c)]: Q_{HC} and Q_{LC} are turned off and on, respectively. v_{LB} in this mode is equal to (4). Therefore, the slope of i_{LB} is identical to that in Mode 2. v_{Lkg} is yielded as

$$v_{Lkg} = -V_{PV} + V_{Cf} + V_{LOAD}/2N. \qquad (6)$$

In this mode, i_{Lkg} increases when $V_{PV} - V_{Cf} < V_{LOAD}/2N$ and vice versa when $V_{PV} - V_{Cf} > V_{LOAD}/2N$. C_f is discharged by $i_{LB} + i_{Lkg}$.
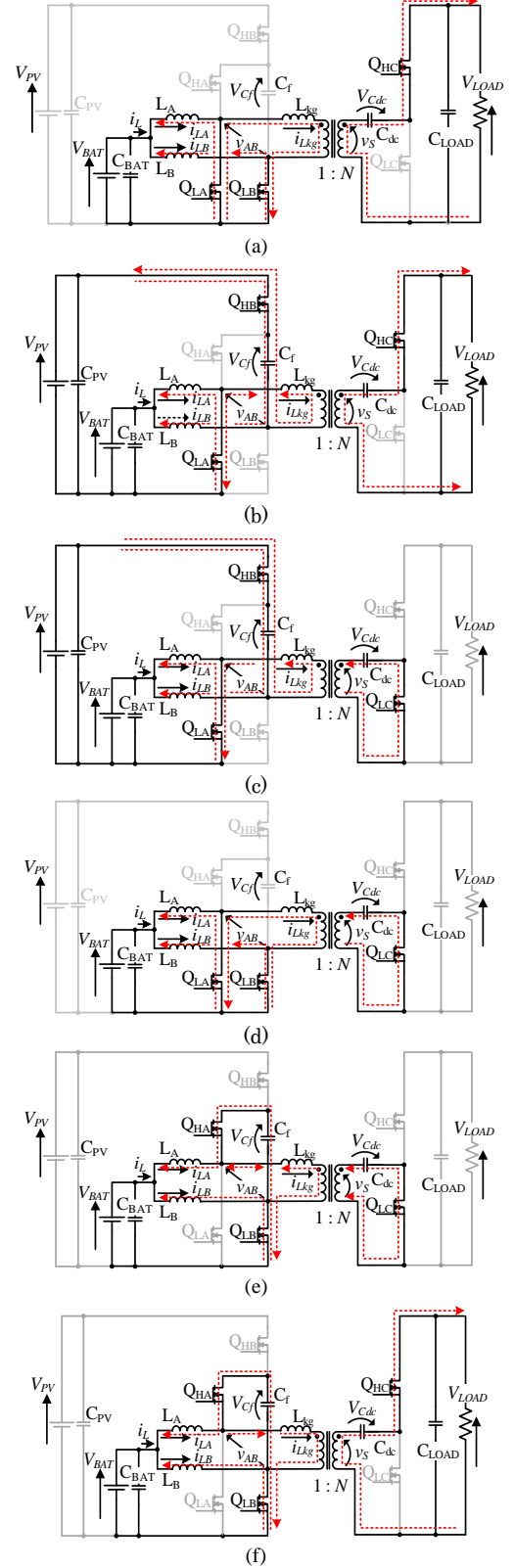

Fig. 5. Current flows in battery charging mode: (a) Mode 1, (b) Mode 2, (c) Mode 3, (d) Mode 4, (e) Mode 5, (f) Mode 6.

Mode 4 (t_3–t_4) [Fig. 5(d)]: Q_{HB} and Q_{LB} are turned off and on, respectively. v_{Lkg} is opposite to that in Mode 1. C_f is neither charged nor discharged in this mode.

Mode 5 (t_4–t_5) [Fig. 5(e)]: Q_{LA} and Q_{HA} are turned off and on, respectively. v_{LA} and v_{Lkg} are

$$v_{LA} = V_{BAT} - V_{Cf} \tag{7}$$

$$v_{Lkg} = V_{Cf} + V_{LOAD}/2N . \tag{8}$$

i_{LA} starts decreasing (as well as Mode 6), while i_{Lkg} increases. In this mode, C_f is charged by $i_{LA} - i_{Lkg}$.

Mode 6 (t_5–t_6) [Fig. 5(f)]: Q_{LC} and Q_{HC} are turned off and on, respectively. v_{Lkg} is expressed as

$$v_{Lkg} = V_{Cf} - V_{LOAD}/2N . \tag{9}$$

i_{Lkg} increases when $V_{Cf} > V_{LOAD}/2N$ and vice versa when $V_{Cf} < V_{LOAD}/2N$. C_f is still charged by $i_{LA} - i_{Lkg}$, similarly to Mode 5.

B. Automatic Current Balancing

As mentioned in Section III-A, C_f is charged by $i_{LA} - i_{Lkg}$ in Modes 5–6 with the length of $(1 - d_A)T_S$ and is discharged by $i_{LB} + i_{Lkg}$ in Modes 2–3 with the length of $(1 - d_B)T_S$. Meanwhile, C_{dc} is charged and discharged by i_{Lkg}. Based on the charge balances on C_f and C_{dc}, following equation is yielded

$$(1-d_A)I_{LA} = (1-d_B)I_{LB} , \tag{10}$$

where I_{LA} and I_{LB} are the average currents of i_{LA} and i_{LB}, respectively. Therefore, under the condition that d_A and d_B are identical, i_{LA} and i_{LB} can be automatically balanced without feedback control loops nor current sensors.

C. Output Characteristics

In the interleaved PWM converter, V_{Cf} can be yielded by applying (2) and (7) to volt-sec balance on L_A, as

$$V_{Cf} = \frac{V_{BAT}}{1-d_A} , \tag{11}$$

Volt-sec balance on L_B with (2) and (4) yields

$$V_{PV} = V_{Cf} + \frac{V_{BAT}}{1-d_B} . \tag{12}$$

Given that each duty cycle is identical as $d_A = d_B = d$, substituting (11) into (12) produces the voltage conversion ratio between V_{PV} and V_{BAT} as

$$\frac{V_{PV}}{V_{BAT}} = \frac{2}{1-d} . \tag{13}$$

Thus, the voltage conversion ratio of the interleaved PWM converter in the proposed MPC is doubled compared with that of the conventional MPCs [7]–[9].

P_{LOAD} can be derived from (3), (5), (8), and (9) by applying volt-sec balance on L_{kg} and charge balance on C_{dc}. P_{LOAD} is expressed by the following equations. When $d > 0.5$,

$$\begin{cases} P_{LOAD} = \dfrac{V_{PV}V_{LOAD}\{d(1-d)+2\varphi_D(1-2\varphi_D)-1/4\}}{8NfL_{kg}} \left(\varphi_D > \dfrac{d}{2}-\dfrac{1}{4}\right) \\ P_{LOAD} = \dfrac{V_{PV}V_{LOAD}\varphi_D(1-d)}{2NfL_{kg}} \left(\varphi_D \le \dfrac{d}{2}-\dfrac{1}{4}\right) \end{cases} . \tag{14}$$

When $d \le 0.5$

$$P_{LOAD} = \frac{V_{PV}V_{LOAD}\varphi_D\{2d(1-d)-\varphi_D\}}{2NfL_{kg}} , \tag{15}$$

where f is the switching frequency.

D. ZVS Conditions

To achieve ZVS turn-on, a body diode of each switch needs to conduct before its gating signal is applied. ZVS constraints for each switch are expressed as

$$\begin{cases} Q_{LA}: i_{LA}(t_0) - i_{Lkg}(t_0) < 0 \\ Q_{LB}: i_{LB}(t_3) + i_{Lkg}(t_3) < 0 \\ Q_{HA}: i_{LA}(t_4) - i_{Lkg}(t_4) > 0 \\ Q_{HB}: i_{LB}(t_1) + i_{Lkg}(t_1) > 0 \\ Q_{LC}: i_{Lkg}(t_2) < 0 \\ Q_{HC}: -i_{Lkg}(t_5) < 0 \end{cases} , \tag{16}$$

$$\rightarrow \begin{cases} Q_{LA}: k < \dfrac{2(1-d)(1+dl_A)+2M(d+2\varphi_D-1)}{d(1-d)+2\varphi_D(1-2\varphi_D)-1/4} \\ Q_{LB}: k < \dfrac{2(1-d)(1+dl_B)+2M(d+2\varphi_D-1)}{d(1-d)+2\varphi_D(1-2\varphi_D)-1/4} \\ Q_{HA}: k > \dfrac{4\varphi_D+M-1+2d(d-1)l_A}{d(1-d)+2\varphi_D(1-2\varphi_D)-1/4} \\ Q_{HB}: k > \dfrac{4\varphi_D+M-1+2d(d-1)l_B}{d(1-d)+2\varphi_D(1-2\varphi_D)-1/4} \\ Q_{LC}, Q_{HC}: \varphi_D > \dfrac{1}{4}(1-M) \end{cases} , \tag{17}$$

where k is the current ratio of the battery current I_{BAT} and load current I_{LOAD} ($k = I_{BAT}/I_{LOAD}$), and M is the voltage conversion ratio ($M = V_{LOAD}/NV_{PV}$). l_A and l_B are the ratio of L_{kg} to L_A ($l_A = L_{kg}/L_A$) and L_{kg} to L_B ($l_B = L_{kg}/L_B$). The ZVS constraints of the primary side switches are determined not only by i_{Lkg} but also i_{LA} or i_{LB}, according to (16). The ZVS boundary of (17) is shown in Fig. 6. It suggests that the ZVS range becomes narrow as k increases. On the other hand, ZVS turn-off can always be achieved for all switches thanks to a parasitic drain-source capacitance of each switch.
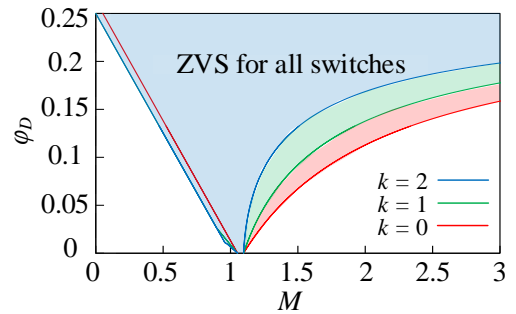

Fig. 6. ZVS boudaries at $d = 0.5$, $l_A = l_B = 0.1$ and $k = 0$–2.

E. Transformer Utilization and Switch Voltage Stress

Fig. 7 compares waveforms of v_{AB} between the proposed and conventional MPCs with $V_{PV}/V_{BAT} = 4.0$. In the conventional MPC, a period of $v_{AB} = 0$ exists because d must be 0.75 to achieve $V_{PV}/V_{BAT} = 4.0$. During this zero-voltage period,
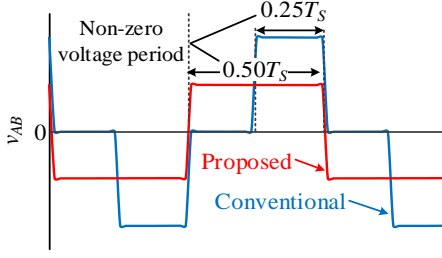
Fig. 7. Voltage across primary winding with $V_{PV}/V_{BAT} = 4.0$.

no power can be transferred through the transformer, resulting in poor transformer utilization and increased RMC current as well as copper loss. The proposed MPC, on the other hand, can extend the non-zero voltage period because the voltage conversion ratio is doubled compared with that of the conventional one. According to (13), the operation with $d = 0.5$ realizes the voltage gain of $V_{PV}/V_{BAT} = 4.0$. Hence, a zero-voltage period can be eliminated, and the transformer utilization can be maximized.

The voltages stresses of Q_{LA}, Q_{LB}, Q_{HA}, and Q_{HB} are expressed as

$$\begin{cases} v_{ds}(Q_{LA}) = V_{Cf} \\ v_{ds}(Q_{LB}) = V_{PV} - V_{Cf} \\ v_{ds}(Q_{HA}) = V_{PV} \\ v_{ds}(Q_{HB}) = V_{PV} - V_{Cf} \end{cases}. \quad (18)$$

The voltage stresses under $d = 0.5$ are derived by substituting (11) and (13) into (18), as

$$\begin{cases} v_{ds}(Q_{LA}) = v_{ds}(Q_{LB}) = v_{ds}(Q_{HB}) = \dfrac{V_{PV}}{2} \\ v_{ds}(Q_{HA}) = V_{PV} \end{cases}. \quad (19)$$

This equation suggests that the voltage stresses of Q_{LA}, Q_{LB}, and Q_{HB} are suppressed to half of V_{PV}.
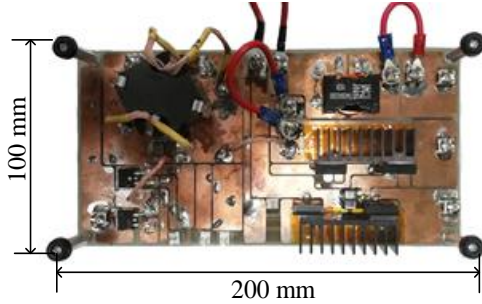

Fig. 8. 300-W prototype.

Table I. Component values.

Items	Values
C_{PV}	Ceramic Capacitor, 100 µF
C_{BAT}	Ceramic Capacitor, 30 µF
C_{LOAD}	Aluminum Electrolytic Capacitor, 360 µF
C_f	Ceramic Capacitor, 40 µF
C_{dc}	Ceramic Capacitor, 6.6 µF
Tr	$N = 4.25$, $L_{kg} = 0.8$ µF, $L_{mg} = 15.7$ µF
L_A, L_B	33 µF, $R_{dc} = 2.4$ mΩ
Q_{LA}, Q_{LB}, Q_{HA}, Q_{HB}	FDH055N15A, $V_{DS} = 150$ V, $R_{on} = 5.9$ mΩ
Q_{LC}, Q_{HC}	SiHB28N60EF, $V_{DS} = 650$ V, $R_{on} = 123$ mΩ
Gate Driver	ADuM3223ARZ

IV. EXPERIMENTAL RESULTS

A. Prototype

A 300-W ($P_{BAT} = 100$ W, $P_{LOAD} = 200$ W) prototype was designed and built for $V_{PV} = 48$ V, $V_{BAT} = 12$ V, and $V_{LOAD} = 200$ V, as shown in Fig. 8, and its switching frequency was 100 kHz. Component values are listed in Table I.

B. Output Characteristics

The measured voltage conversion ratio of V_{PV}/V_{BAT} is shown in Fig. 9(a). V_{PV}/V_{BAT} were dependent only on d, suggesting that the operation of the interleaved PWM converter was independent on PS control. Fig. 9(b) shows measured P_{LOAD} characteristics as a function of φ. P_{LOAD} was dependent on both d and φ, suggesting an existence of the cross-regulation issue between PWM and PS controls. The interdependence would be eliminated by introducing a decoupling network [10], [11], which will be a part of our future works.
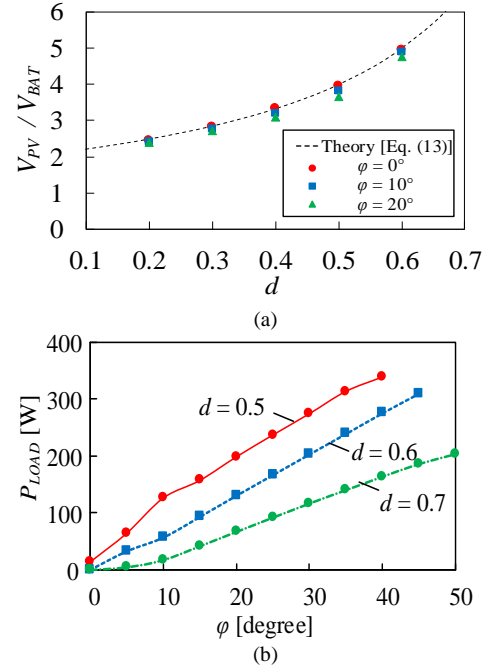

(a)

(b)

Fig. 9 Measured output characteristics at $V_{PV} = 48$ V, $V_{BAT} = 12$ V, and $V_{LOAD} = 200$ V: (a) V_{PV}/V_{BAT} as a function of d [Eq. (13)], (b) P_{LOAD} as a function of φ.

C. Measured Waveforms

Measured voltage waveforms of switches on the primary side (Q_{LA}, Q_{LB}, Q_{HA}, and Q_{HB}) in the battery charging mode are shown in Fig. 10(a). Thanks to C_f, v_{ds} of Q_{LA}, Q_{LB}, and Q_{HB} were suppressed to around half the input voltage of 48 V, reducing voltage stresses compared with those of the conventional MPCs [7]–[9].

The measured waveforms of v_{AB}, i_{LA}, i_{LB}, and i_{BAT} are shown in Fig. 10(b). There was no zero-voltage period of v_{AB} at the condition of $V_{PV}/V_{BAT} = 4.0$, meaning the transformer utilization was improved compared with those of conventional MPCs. i_{LA} and i_{LB}, were automatically balanced, and the current ripple of the battery port was canceled.
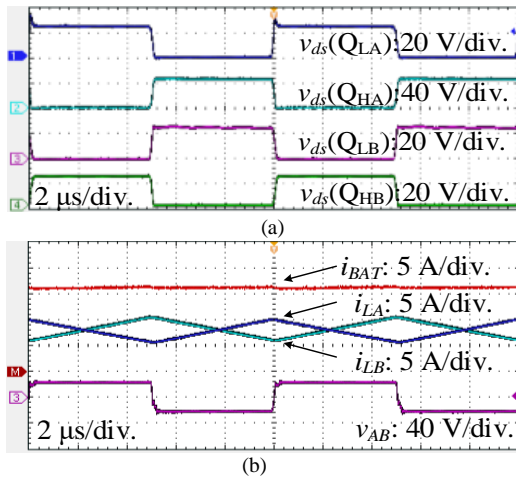
Fig. 10. Measured waveforms in battery charging mode at V_{PV} = 48 V, V_{BAT} = 12 V, V_{LOAD} = 200 V, d = 0.5, and φ = 20°. (a) v_{ds} (Q$_{LA}$, Q$_{LB}$, Q$_{HA}$ and Q$_{HB}$) and (b) i_{BAT}, i_{LA}, i_{LB}, v_{AB}.
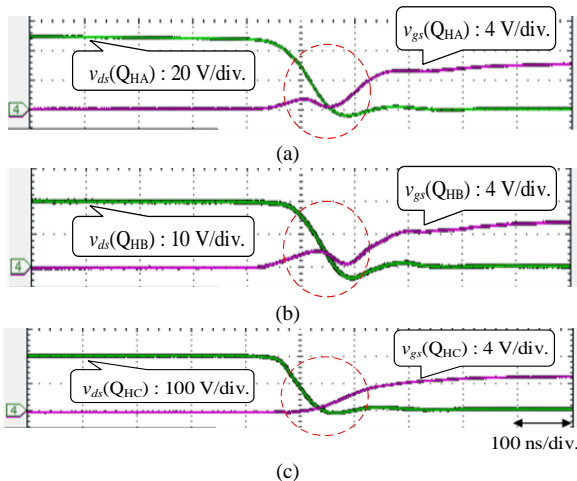

Fig. 11. Measured v_{gs} and v_{ds} at P_{LOAD} = 300 W. (a) Q$_{HA}$, (b) Q$_{HB}$, (c) Q$_{HC}$.

The measured waveforms of v_{ds} and v_{gs} at a full load of 300 W are shown in Fig. 11. v_{ds} dropped to almost zero before applying v_{gs}, verifying ZVS operations for all switches.

D. Power Conversion Efficiency and Loss Analysis

The measured power conversion efficiencies in the battery charging mode at fixed values of P_{BAT} are shown in Fig. 12. The peak efficiency at a full load was as high as 94.4%. The power conversion efficiency consistently increased with P_{BAT}, suggesting that the efficiency of the interleaved PWM converter was higher than that of the DAB converter.

V. CONCLUSION

This paper has proposed the MPC integrating the automatic current balancing interleaved PWM converter and DAB converter with a high transformer utilization. The detailed operation analysis was performed to derive the output characteristics in the battery charging mode. In addition, the improved transformer utilization and current balancing principle were described.

The experimental results using the 300-W prototype verified that two inductor currents were automatically balanced
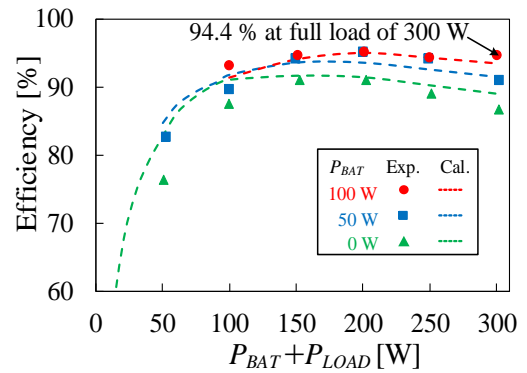

Fig. 12. Measured power conversion efficiencies in battery charging mode.

without feedback control, and the transformer utilization was improved compared with that in the conventional MPCs. The measured power conversion efficiency in the battery charging mode was as high as 94.4% at the full load of 300 W. The loss analysis revealed that reduction in the copper loss of the transformer windings and employing low-resistance capacitor would effectively improve the power conversion efficiency in the heavy load region.

REFERENCES

[1] J. L. Duarte, M. Hendrix, and M. G. Simoes, "Three-port bidirectional converter for hybrid fuel cell systems," *IEEE Trans. Power Electron.*, vol. 22, no. 2, pp. 480–487, Mar. 2007.

[2] C. Zhao, S. D. Round, and J. W. Kolar, "An isolated three-port bidirectional dc–dc converter with decoupled power flow management," *IEEE Trans. Power. Electron.*, vol. 23, no. 5, pp. 2443–2453, Sep. 2008.

[3] H. Nagata and M. Uno, "Multi-port converter integrating two PWM converters for multi-power-source systems," in *Proc. Int. Future Energy Electron. Conf. 2017 (IFEEC 2017)*, pp. 1833–1838, Jun. 2017.

[4] M. Uno and K. Sugiyama, "Switched capacitor converter based multiport converter integrating bidirectional PWM and series-resonant converters for standalone photovoltaic systems," *IEEE Trans. Power Electron.*, vol. 34, no. 2, pp. 1394–1406, Feb. 2019.

[5] G. Su and L. Tang, "A multiphase, modular, bidirectional, triple-voltage dc–dc Converter for hybrid and fuel cell vehicle power systems" *IEEE Trans. Ind. Electron.*, vol. 23, no. 6, pp. 3035–3046, Nov. 2008.

[6] Q. Wang, J.Zhang, X. Ruan and K. Jin, "Isolated single primary winding multiple-input converters" *IEEE Trans. Ind. Electron.*, vol. 26, no. 12, pp. 3435–3442, Dec. 2011.

[7] J. Zhang, H. Wu, X. Qin, and Y. Xing, "PWM plus secondary-side phase-shift controlled soft-switching full-bridge three-port converter for renewable power systems," *IEEE Trans. Power Electron.*, vol. 62, no. 11, pp. 7061–7072, Nov. 2015.

[8] W. Li, X. Yi Zhao, and X He, "PWM plus phase angle shift (PPAS) control scheme for combined multiport dc/dc converters", *IEEE Trans. Power Electron.*, vol. 27, no. 3, pp. 1479–1489, Mar. 2012.

[9] M. Mira, Z. Zhang, A. Knott, and M. Anderson, "Analysis, design, modeling, and control of an interleaved-boost full-bridge three-port converter for hybrid renewable energy systems", *IEEE Trans. Power Electron.*, vol. 32, no. 2, pp. 1138–1155, Feb. 2017.

[10] Z. Qian, O. A. Rahman, H. A. Atrach, and I. Batarseh, "Modeling and control of three-port dc/dc converter interface for satellite applications," *IEEE Trans. Power Electron.*, vol. 25, no. 3, pp. 637–649, Mar. 2010.

[11] C. Zhao, S. D. Round, and J. W. Kolar, "An isolated three-port bidirectional dc–dc converter with decoupled power flow management," *IEEE Trans. Power Electron.*, vol. 23, no. 5, pp. 2443–2453, Sep. 2008.